frontiers | Frontiers in Nutrition

TYPE Original Research
PUBLISHED 09 December 2022
DOI 10.3389/fnut.2022.1061552

OPEN ACCESS

EDITED BY
Simon McArthur,
Queen Mary University of London,
United Kingdom

REVIEWED BY
Kamila Borowiec,
University of Life Sciences of
Lublin, Poland
Jessie Gutierres,
Federal University of Health Sciences
of Porto Alegre, Brazil

*CORRESPONDENCE
Lin Zhang
zhanglin840514@126.com

SPECIALTY SECTION
This article was submitted to
Nutrition, Psychology and Brain
Health,
a section of the journal
Frontiers in Nutrition

RECEIVED 04 October 2022
ACCEPTED 17 November 2022
PUBLISHED 09 December 2022

CITATION
Xiao R, Liang R, Cai Y-h, Dong J and
Zhang L (2022) Computational
screening for new neuroprotective
ingredients against Alzheimer's disease
from bilberry by cheminformatics
approaches. *Front. Nutr.* 9:1061552.
doi: 10.3389/fnut.2022.1061552

Computational screening for new neuroprotective ingredients against Alzheimer's disease from bilberry by cheminformatics approaches

Ran Xiao[1,3], Rui Liang[1], Yun-hui Cai[1], Jie Dong[2] and Lin Zhang[1]*

[1]Hunan Key Laboratory of Processed Food for Special Medical Purpose, Hunan Key Laboratory of Forestry Edible Resources Safety and Processing, School of Food Science and Engineering, National Engineering Research Center of Rice and Byproduct Deep Processing, Central South University of Forestry and Technology, Changsha, China, [2]Xiangya School of Pharmaceutical Science, Central South University, Changsha, China, [3]Sinocare Inc., Changsha, China

Bioactive ingredients from natural products have always been an important resource for the discovery of drugs for Alzheimer's disease (AD). Senile plaques, which are formed with amyloid-beta (Aβ) peptides and excess metal ions, are found in AD brains and have been suggested to play an important role in AD pathogenesis. Here, we attempted to design an effective and smart screening method based on cheminformatics approaches to find new ingredients against AD from *Vaccinium myrtillus* (bilberry) and verified the bioactivity of expected ingredients through experiments. This method integrated advanced artificial intelligence models and target prediction methods to realize the stepwise analysis and filtering of all ingredients. Finally, we obtained the expected new compound malvidin-3-O-galactoside (Ma-3-gal-Cl). The *in vitro* experiments showed that Ma-3-gal-Cl could reduce the OH· generation and intracellular ROS from the Aβ/Cu^{2+}/AA mixture and maintain the mitochondrial membrane potential of SH-SY5Y cells. Molecular docking and Western blot results indicated that Ma-3-gal-Cl could reduce the amount of activated caspase-3 *via* binding with unactivated caspase-3 and reduce the expression of phosphorylated p38 *via* binding with mitogen-activated protein kinase kinases-6 (MKK6). Moreover, Ma-3-gal-Cl could inhibit the Aβ aggregation *via* binding with Aβ monomer and fibers. Thus, Ma-3-gal-Cl showed significant effects on protecting SH-SY5Y cells from Aβ/Cu^{2+}/AA induced damage *via* antioxidation effect and inhibition effect to the Aβ aggregation.

KEYWORDS

anthocyanins, Alzheimer's disease, cheminformatics, antioxidation, anti-aggregation

Introduction

Alzheimer's disease (AD) is a chronic neurodegenerative disease (1), which is most commonly associated with dementia in elderly people. Its clinical symptoms usually include memory loss, cognitive impairment, and behavioral dysfunction. The characteristic pathological changes in AD include cerebral atrophy, amyloid plaques, and neurofibrillary tangles in the brains of patients. The pathology of AD shows a significant correlation between amyloid-beta (Aβ) protein and the clinical severity of dementia (2). The amyloid cascade hypothesis indicates that the Aβ aggregates that self-assembled from misfolded Aβ can affect the structure and functions of neuronal cells and induce cell apoptosis, leading to synaptic dysfunction and neurodegeneration (3). Aβ peptides of 39–43 amino acids are a kind of hydrolysate of the transmembrane glycoprotein β amyloid precursor protein (APP). Among these Aβ peptides, Aβ (1–42) has the most prone to self-aggregate and generate neurotoxic aggregates (e.g., oligomers and fibers) (4). Meanwhile, the excess of copper ions (Cu^{2+}) (∼0.4 mmol/L), which were found in the senile plaque, were reported to induce oxidative stress in the AD brain, which is also an important cause of neurotoxicity (5, 6). Under a normal physiological environment, Aβ cannot self-aggregate due to the low concentration (5). However, in the pathological environment, Aβ concentration was increased that induced it to self-aggregate. At the same time, Cu^{2+} could bind to Aβ and form the Aβ-Cu^{2+} complex, which could react with ascorbic acid (AA) (500 μmol/L−10 mmol/L) in the brain to continuously generate excessive hydroxyl radicals (OH·) and reactive oxygen species (ROS) *via* Fenton and Harber–Weiss reactions (7). These ROS radicals will further increase the damage to neurons and aggravate the progression of AD (8).

Based on these mechanisms, many attempts have been made to discover new drugs that may intervene in these processes to relieve the symptoms of AD (9). There is no doubt that natural products provide abundant bioactive molecules for pharmaceutical chemists to screen and find suitable active ingredients and promote them to promising lead compounds further (10, 11). Anthocyanins, a category of polyhydroxy or polymethoxy derivatives of 2-phenylbenzopyran cations (12, 13), can be found in high abundance in natural plants. The main structure of anthocyanins contains two substituted benzene rings separated by an oxygen-containing heterocycle (14). According to the number and position of the substituents, 635 anthocyanins have been identified (14). The most common anthocyanins in natural plants are pelargonidin, cyanidin, peonidin, delphinidin, petunidin, and malvidin (13). In recent years, studies have shown that anthocyanins can show a variety of biological activities such as antioxidant, anti-inflammatory, and anti-apoptosis (15, 16). It has been pointed out that long-term dietary supplementation with anthocyanins can help reverse age-related cognitive deficits and neurological functions (17, 18). Furthermore, several studies have shown that anthocyanins can delay the occurrence and development of AD by inhibiting Aβ aggregation, neural cell apoptosis, and anti-inflammatory and antioxidation effects (17, 18). A berry plant rich in anthocyanins, *Vaccinium myrtillus* (bilberry), has attracted our interest. Therefore, an effective strategy was expected to find ingredients unreported that may fight against AD.

Cheminformatics is a new interdisciplinary technology with rapid growth in recent years. In the field of drug discovery, many cheminformatics methods such as physical and chemical property calculation, quantitative structure–activity relationship research (QSAR), similarity calculation, and scaffold hopping have been widely used in drug absorption, distribution, metabolism, excretion, and toxicity (ADMET) prediction, drug target prediction, and virtual screening of new molecular entities (19–21). In the field of food, cheminformatics methods are also gradually used in flavor prediction, food traceability, food fraud, and food detection (22–25). Especially, they have been more and more widely applied in the studies of discovering unreported compound entities and interpreting unconfirmed biological mechanisms from plants or foods (26, 27). Techniques based on cheminformatics can make full use of the information-processing ability of computers and quickly find answers from the vast chemical space. This will not only help researchers get the results quickly but also avoid knowledge-based one-sidedness at different levels of understanding.

In this study, we expect to design an efficient computational method based on cheminformatics to find the expected ingredients from bilberry. First, we need to collect all the chemical ingredients in bilberry and filter out the molecules that obviously did not meet the requirements by calculating the basic physical and chemical properties. Then, based on the advanced artificial intelligence models, a reasonable filter rule should be constructed, and the ingredients with essential drug-likeness properties in bilberry will be selected by scoring and sorting. Next, several advanced target prediction methods will be employed to predict the interaction between the ingredients and important targets related to AD. Through knowledge-based analysis and discrimination, the relevant ingredients that may show good possibility against AD are expected to be found. According to the molecular mechanisms of the pathogenesis and progress of AD, reasonable *in vitro* experiments will be designed to further verify the biological activity of the screened ingredients. Molecular docking will be subsequently used to simulate the docking of the validated ingredients to further elaborate the possible mechanism of action.

Materials and methods

Cheminformatics approaches

All the ingredients of bilberry were collected from the FooDB database (https://foodb.ca/, Version 1.0). The basic physical and chemical properties were calculated using ChemDes (28) and PyBioMed (29) toolkits, which were widely used in the drug design and enabled quick calculation of a variety of molecular descriptors. The properties used here included molecular weight (MW), number of hydrogen bond receptors (nHA), number of hydrogen bond donors (nHD), number of rotatable bonds (nRot), number of rings (nRing), and formal charge (fChar).

The ADMET prediction was conducted using ADMETlab (Version 1.0 and 2.0) (20, 30), which was the famous platform for early ADMET evaluation in drug development. The ADMET indicators used here included LogP, hERG, H-HT, Ames, ROA, Carcinogenicity, Respiratory, Non-Genotoxic_Carcinogenicity, and Genotoxic_Carcinogenicity_Mutagenicity. A detailed explanation of these indicators can be found at https://admetmesh.scbdd.com/explanation/index. By using KNIME software and Python programming, the rules for filtering ingredients are set as shown in Supplementary Figure S1. By sorting the calculated ADMET scores, the best ones will be listed at the top.

To construct a reasonable pipeline for the target prediction, we first reviewed publications and found that Aβ (1–42) (UniProt ID: P05067), AChE (P22303), and caspase-3 (UniProt ID: P42574) could be three important targets though they act as different roles in different Alzheimer's hypotheses. Then, we tried to search for target prediction tools driven by advanced artificial intelligence. SEA (31), SwissTargetPrediction (32), TargetNet (21), PPB2 (33), PharmMapper (34, 35), and SuperPred (36, 37) were employed to perform the target prediction for ingredients refined after the ADMET filtering, since this step was a rough prediction, and the scoring standards varied between different tools. At the same time, more possibilities were expected to be seen. We set a relatively loose threshold, that is, the first 20 hits were retained and then forwarded to analysis.

Experimental materials

Ma-3-gal-Cl (cat. no. IP-0246) was purchased from Shanghai Tauto Biotechnology Co., Ltd. (Shanghai, China). Fetal bovine serum (FBS) (cat. no. 10270-106), Dulbecco's Modified Eagle Media: Nutrient Mixture F-12 (DMEM/F12) (1:1) (cat. no. C11330500BT), and 0.25% trypsin (cat. no. 25200-056) were purchased from Gibco (CA, USA). Aβ (1–42) (cat. no. 107761-42-2) for atomic force microscopy was purchased from American Peptide Company, Inc. (California, American). Active oxygen detection kit (cat. no. S0033S) and mitochondrial membrane potential detection kit 5,5′,6,6′-Tetrachloro-1,1′,3,3′-tetraethyl-imidacarbocyanine (JC-1) (cat. no. C2006) were obtained from Beyotime Biological Reagent Co., Ltd (Shanghai, China). Coumarin-3-carboxylic acid (CCA) (cat. no. C85603), ascorbic acid (AA) (cat. no. A800296), 3-(4,5-Dimethylthiazol-2-yl)-2,5-diphenyltetrazolium bromide (MTT) (cat. no. M2003), $CuSO_4$ (cat. no. 209198), 30% H_2O_2 (cat. no. 10011208), and other reagents were purchased from Sigma-Aldrich Co. (St Louis, MO, USA). Cleaved caspase-3 (1: 1000, cat. no. ARG57512) and P-p38 (1: 500, cat. no. ARG51850) were obtained from Arigo (Hsinchu City, Taiwan, China), and p38 (1: 1000, cat. no. #9212) was obtained from Cell Signaling Technology (Danvers, MA, USA). The Ma-3-gal-Cl was first dissolved in DMSO (2 mmol/L). Then, it will be diluted to different concentrations by cell culture medium of DMEM/F12 (1:1) in cell-related experiments and ultrapure water in other experiments for further use. The Aβ (1–42) powder was first dissolved in 20 mmol/L NaOH to get the concentration of 500 μmol/L and then diluted to different concentrations by DMEM/F12 in cell-related experiments and PBS (pH = 7.4) in other experiments for further use. CCA powder was dissolved in PBS (20 mmol/L, pH = 9.0) and then adjust the pH to 7.4 with KH_2PO_4 solution, and the CCA concentration was calculated as 5 mmol/L. Thioflavin (ThT) was prepared into a concentration of 5 μmol/L by PBS (10 mmol/L, pH = 7.4).

Cell viability assays

The undifferentiated human neuroblastoma cell line (SH-SY5Y) is a commonly used neuronal cell model for Alzheimer's disease (38–40). Undifferentiated SH-SY5Y was purchased from USA ATCC Company (Washington, DC, USA). SH-SY5Y cells were cultured in DMEM/F12 (1:1) basic medium containing 10% FBS and 1% penicillin and streptomycin mixture in a cell incubator under 5% CO_2 at 37°C. The well-cultured cells were transferred to a sterile 96-well plate with approximately 1×10^4 cells/well. Aβ (1–42), Aβ (1–42)/Cu/AA, or Ma-3-gal-Cl solutions were mixed and incubated with the SH-SY5Y cells for 24 h. The viability of the SH-SY5Y cells exposed to each solution was determined with an MTT assay.

Detection of hydroxyl radical

Coumarin-3-carboxylic acid was used as a fluorescence probe for OH· determination (41) with a Hitachi F-4600 spectrofluorometer from Hitachi High-Tech Corporation (Tokyo, Japan). CCA fluorescence was recorded at 540 nm, with an excitation wavelength of 390 nm. The widths of the entrance and exit slits were both 5 nm. The OH·amounts in the solutions of Aβ (1–42) (10 μmol/L)/Cu^{2+} (5 μmol/L)/AA (1 mmol/L)

mixture in the presence or absence of different concentrations of Ma-3-gal-Cl (0.5, 4, and 10 μmol/L) were detected with CCA probe. The fluorescence ratio was calculated as follows:

$$\text{Ratio}\ (\%) = 100 \times F/F_0 \quad (1)$$

Where F is the CCA fluorescence intensity in each solution, and F_0 is the CCA fluorescence intensity of the Aβ (1–42) (10 μmol/L)/Cu^{2+} (5 μmol/L)/AA (1 mmol/L) mixture.

Intracellular reactive oxygen species determination

DCFH-DA was used to detect the level of intracellular reactive oxygen species (ROS). The SH-SY5Y cells were treated with different solutions for 24 h and then treated according to the instruction of the DCFH-DA kit. The fluorescence intensity was recorded with the Hitachi F-4600 spectrofluorometer from Hitachi High-Tech Corporation (Tokyo, Japan) with the excitation and emission wavelengths at 485 nm and 525 nm. The fluorescence ratio was calculated as follows:

$$\text{Ratio}\ (\%) = 100 \times F/F_0 \quad (2)$$

Where *F* is the DCFH-DA fluorescence intensity of Aβ (1–42) (10 μmol/L)/Cu^{2+} (5 μmol/L)/AA (1 mmol/L)/Ma-3-gal-Cl (0.5, 4, 10 μmol/L) mixtures treated SH-SY5Y cells, and F_0 is the DCFH-DA fluorescence intensity of the Aβ (1–42) (10 μmol/L)/Cu^{2+} (5 μmol/L)/AA (1 mmol/L) treated SH-SY5Y cells.

Mitochondrial membrane potential determination

Fluorescent probe JC-1 was used for detecting the mitochondrial membrane potential (MMP) of SH-SY5Y cells. After the incubation treatment, the cells were treated with JC-1 dye following the instruction of the JC-1 kit. The fluorescence intensity was recorded with a DNM-9602 microplate reader from Plan New Technology Co., Ltd. (Beijing, China), and the MMP was calculated as the ratio of JC-1 monomer (FI 530)/JC-1 aggregate (FI 590) fluorescence intensity (42).

Western blot analysis

Proteins were extracted from pretreated SH-SY5Y cells, and protein level was measured with a BCA protein quantification assay kit [Labgic Technology Co., Ltd. (Hefei, China)]. Proteins (8–12 μg/μL) were mixed with equal volume (8–12 μL) of sodium dodecyl sulfate (SDS) buffer (0.125 mol/L Tris-HCl, pH 6.8, 2% SDS, 0.5% 2-mercaptoethanol, 1% bromophenol blue, and 19% glycerol) and boiled for 5 min. Proteins were separated by SDS-polyacrylamide gel and transferred to nitrocellulose membranes. Then, the membranes were incubated with caspase-3 (cleaved), p38, and P-p38 antibodies overnight at 4°C, probed with horseradish peroxidase-conjugated secondary antibodies at room temperature, and imaged with Gel Imager 721-BR10883 from BIO-RAD Co., Ltd. (Hercules, CA, USA).

ThT assays

Thioflavin was used for detecting the aggregation process of Aβ (1–42). The ThT fluorescence intensity of Aβ (1–42) (80 μmol/L) incubated with or without Ma-3-gal-Cl (10 μmol/L) at different times (0, 2, 4, 6, 12, 24, 48, 72, and 96 h) was detected with a Hitachi F-4600 spectrofluorometer (Hitachi, Japan) with the excitation and emission wavelengths of 450 and 490 nm, respectively. The widths of the entrance and exit slits were both 10 nm. The concentration of ThT was 5 μmol/L.

Atomic force microscopy

Atomic force microscopy (AFM) can be used to observe the surface structure of Aβ (1–42) aggregates (43, 44). In this experiment, morphologies of Aβ (1–42) aggregates were characterized with a Nanoman vs. AFM (Bruker, Germany) with tapping mode. Aβ (1–42) was pretreated with hexafluoro-isopropyl alcohol (HFIP) and freeze-dried into powder. The freeze-dried powder was dissolved with 20 mmol/L NaOH and diluted into the experimental concentration with 10 mmol/L PBS buffer (pH 7.4) solution. Samples taken from incubated Aβ (1–42) solutions or Aβ (1–42)/Ma-3-gal-Cl mixtures were dropped on Ni^{2+}-treated mica sheets, briefly washed with ultrapure water, and eventually dried under the gentle nitrogen stream.

Molecular docking

The docking studies were performed using Molecular Operating Environment (MOE) software (version 2019). Before the docking study, we first prepared the Ma-3-gal-Cl by searching the conformation using the default parameters. Then, for proteins, water molecules, ions, and non-standard amino acid residues were detached from the proteins and the hydrogen atoms were added under an AMBERT10 force field. After the automated correction of protein structure using the "Structure Preparation" module, the binding sites were detected. For caspase-3, crystal structure 2J33 (PDB ID: 2J33) (45) was selected

as the unactivated model, and the binding sites were selected according to the original ligand. For the crystal structure of MKK6 (PDB ID: 3VN9) (46), the prior site could be ATP binding site. For the Aβ crystal structure of monomer (PDB ID: 1IYT) (47) and fibril (PDB ID: 2BEG) (48), we scanned the whole surface to find better sites. The prepared Ma-3-gal-Cl was then flexibly docked into the receptor using the "Triangle Matcher" placement method and "London dG" scoring with other default parameters. Finally, ten docking poses were obtained, and the one with the best score was chosen for analysis.

Statistical analysis

The results were calculated using the SPSS l7.0 statistical analysis, and Origin was used for drawing. Each experiment and each group of data were repeated three times. The results were expressed by mean ± standard deviation (mean ± SD), and the single-sample *t*-test was used to compare the group differences. $P < 0.05$ indicated a statistical difference.

Results

Basic screening of drug-likeness ingredients

From the FooDB database, 4,143 components of bilberry were collected. From these components, glycerol and fatty acids such as triglyceride (TG), diacylglycerol (DG), and phosphatidyl ethanolamine (PE) were preliminarily deleted, and 182 ingredients were obtained. After removing 38 entries such as water, inorganic substances, and triglycerides, 144 ingredients were obtained. Next, we retained the ingredients with a molecular weight of <100 because compounds with very small molecular weights always behave without specificity. After this, 132 ingredients were retained for the next analysis.

The 132 ingredients were then fed into the pipeline for ADMET and drug-likeness screening. As the process described in the Python code (Supplementary Figure S1), this step adopted the strategy of a cumulative score. Each ingredient got an inherent score according to whether the properties meet the requirements, and finally each ingredient got a total score. After ranking the total scores, we get the top 10 ingredients. The structures of these 10 ingredients are listed in Supplementary Table S1. We found that delphinidin (49), cyanidin (50), petunidin (51), quercetin (52), gallocatechin (53), epigallocatechin (54), and myricetin (55) all have been reported to relate with their function against AD, while ingredients based on Malvidin scaffold seem no specific reports. This led to our way of thinking: can we make further study of malvidin-3-O-galactoside (Malvidin scaffold) to see whether it is a neuroprotective ingredient that will help to complete a full profile of the bilberry against AD?

Prediction and selection of ingredients against AD

The target prediction results are shown in Figure 1. The simple network displaying the interaction between the top 10 compounds including Ma-3-gal-Cl and the three targets was constructed as shown in Figure 1B. The top 10 compounds all process the possibility that could be interacted with the targets, which was somehow confirmed by the publications mentioned above. For Ma-3-gal-Cl (number C_26), Aβ (1–42) (P05067), Caspase-3 (P42574), and AChE (P22303) were predicted as its targets. To enhance the reliability, we compared the prediction results of different tools. From Figures 1C,D, we observe that TargetNet and SwissTargetPrediction voted the Ma-3-gal-Cl to interact with Aβ (1–42), and TargetNet, SwissTargetPrediction, and PPB2 voted the Ma-3-gal-Cl to interact with AChE. Although the unified prediction criteria and degree of different tools cannot be implemented, the voting results will provide evidence of interaction from multiple perspectives (e.g., similarity, pharmacophore, and chemical genomics). This increased our confidence in exploring its mechanisms against AD related to these two targets.

In AD patients' brains, Aβ was complexed with excess metal (such as copper, iron, and aluminum) ions in senile plaques. It was reported that the Aβ-metal complex, especially the Aβ-Cu^{2+} complex, can facilitate the generation of H_2O_2 by reacting with cellular species such as AA and O_2 (56, 57). In the cellular milieu, any rogue Cu^{2+} that is not readily complexed by Aβ will also react with H_2O_2 to produce hydroxyl radicals *via* the Harber–Weiss reaction and induce oxidative stress to neurons. Meanwhile, the toxic Aβ aggregates are also one of the culprits for neuron apoptosis. According to the cheminformatics results, Ma-3-gal-Cl could interact with Aβ, which suggested that Ma-3-gal-Cl may influence Aβ-Cu^{2+} induced oxidative stress to cells and the formation of the toxic Aβ aggregates. Thus, *in vitro* experiments were performed.

The inhibitory effect of Ma-3-gal-Cl on oxidative damage induced SH-SY5Y cell apoptosis

H_2O_2 is an important reactive oxygen species (ROS), and it is also a precursor for other ROS (e.g., HO). In order to explore the protective effect of Ma-3-gal-Cl on oxidative damage of H_2O_2 to SH-SY5Y cells, SH-SY5Y cells were incubated with different concentrations of Ma-3-gal-Cl and H_2O_2 for 24 h, and the cell viability of SH-SY5Y cells was detected by MTT assay.

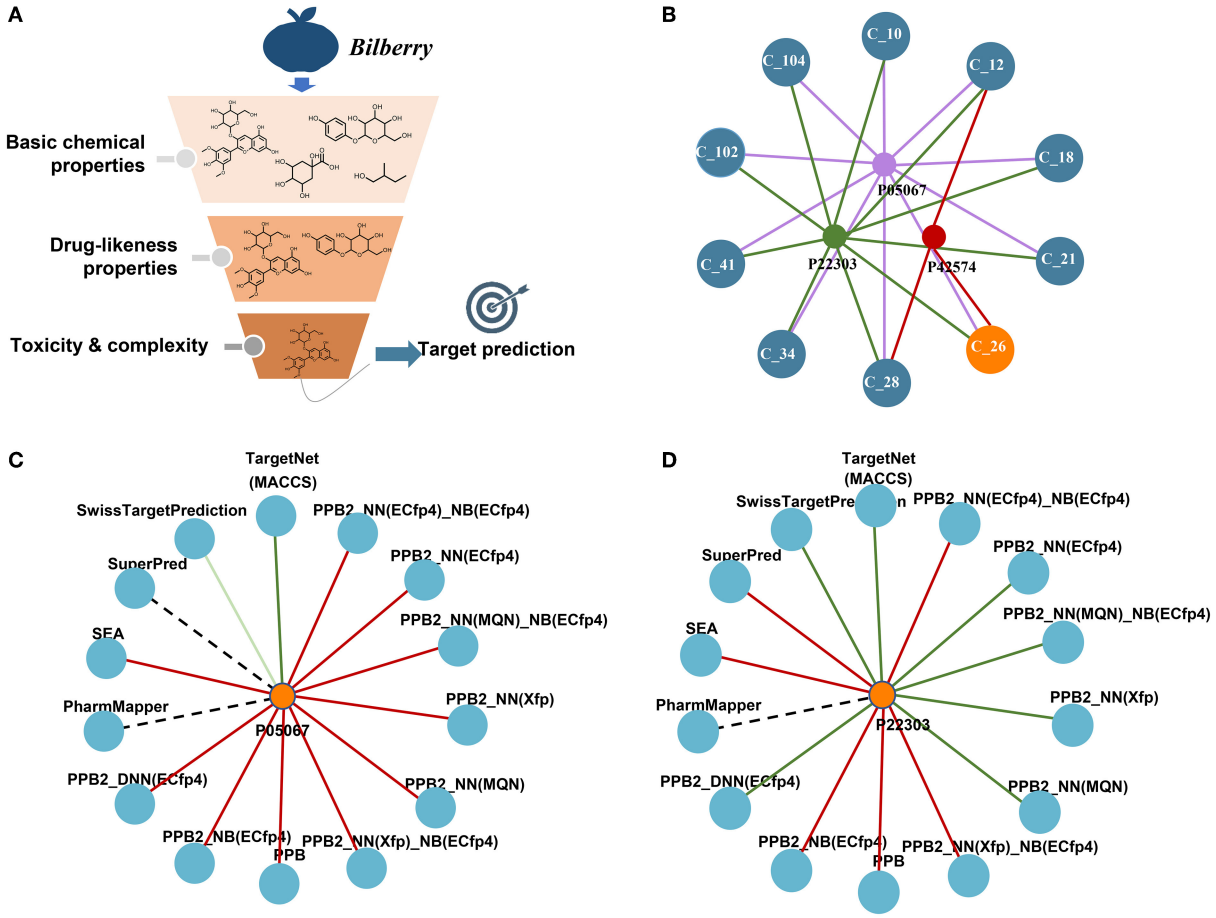

FIGURE 1
Screening of neuroprotective ingredients by cheminformatics approaches. **(A)** The schema of the pipeline. **(B)** The predicted targets and their interactions with the top 10 compounds. C_26 represents Ma-3-gal-Cl. **(C)** The predicted interactions between Ma-3-gal-Cl and Aβ (1–42) by different tools. The red line represents no hit, the dark green represents a hit, and the light green line represents a hit out of the top 20. The dotted line means the tool does not cover this target. **(D)** The predicted interactions between Ma-3-gal-Cl and AChE by different tools.

The results showed that Ma-3-gal-Cl could effectively improve the cell viability of SH-SY5Y cells treated with H_2O_2. When the concentration of Ma-3-gal-Cl increased from 0 to 10 μmol/L, the cell viability was increased from 48.2 to 87.3% ($P < 0.01$) (Figure 2B). Additionally, when the concentration of Ma-3-gal-Cl increased to 20 μmol/L, the cell viability was decreased to 77.6%. These results indicated that Ma-3-gal-Cl with a lower concentration (below 10 μmol/L) could effectively inhibit the H_2O_2–induced cell apoptosis. But at the high concentration of Ma-3-gal-Cl (20 μmol/L), due to the cell toxicity of Ma-3-gal-Cl, lower cell viability was observed (Supplementary Figure S2).

In the senile plaques of patients with AD, large amounts of redox-active metal ions such as Cu^{2+} and Fe^{2+} have been found to coexist with the aggregates of amyloid-beta (Aβ) peptides (58). These metal ions can strongly bind Aβ peptides (58, 59), and the resultant complexes can facilitate the generation of H_2O_2 by reacting with cellular species such as AA and O_2 (59). Furthermore, redox metal ions (e.g., Cu^{2+} and Fe^{2+}) can generate hydroxyl radicals (OH•) by reacting with H_2O_2 through the Harber–Weiss and Fenton reactions (8, 60). Thus, in this study, the Aβ (1–42)/Cu^{2+}/AA system was used as the OH• production model to simulate the OH• producing process in senile plaques of patients with AD.

To investigate the inhibition effect of Ma-3-gal-Cl to Aβ (1–42)/Cu^{2+}/AA induced cell apoptosis, the cell viability of SH-SY5Y cells incubated with different concentrations of Ma-3-gal-Cl/Aβ (1–42)/Cu^{2+}/AA mixture was detected. As shown in Supplementary Figure S3, the low concentrations of Cu^{2+} (5 μmol/L) or AA (1 mmol/L) alone showed no cell toxicity to SH-SY5Y cells. Aβ (1–42) (10 μmol/L) reduced the cell viability to 92.3% (Supplementary Figure S3). However, when the same concentration of Aβ (1–42), Cu^{2+}, and AA was mixed, the cell viability was decreased to 55.0%. This may be due to the oxidative damage from OH· produced by Aβ (1–42)/Cu^{2+}/AA

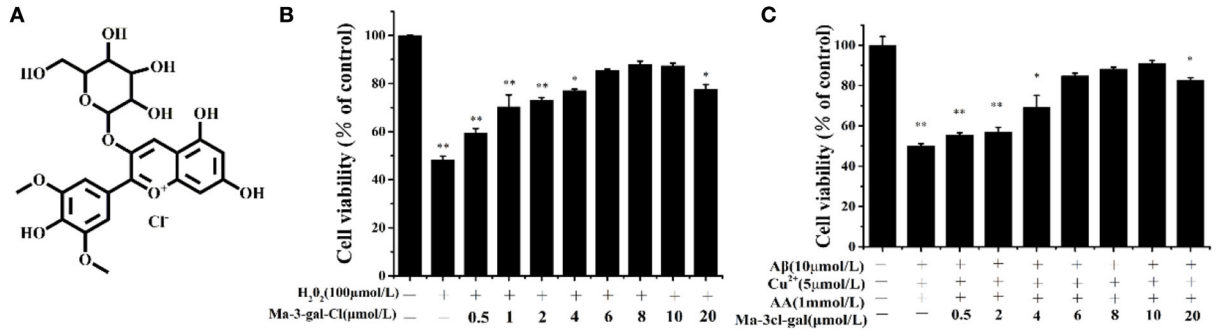

FIGURE 2
Molecular structure of Ma-3-gal-Cl **(A)**, and cell viability of SH-SY5Y cells treated with different solutions **(B,C)**. $^{*}p < 0.05$ and $^{**}p < 0.01$ compared to control values.

system, and the cell toxicity from Aβ (1–42) toxic aggregates. As shown in Figure 2C, when the concentration of Ma-3-gal-Cl increased from 0 to 10 μmol/L, the cell viability was increased from 55.0% to 90.9%. When the concentration of Ma-3-gal-Cl increased to 20 μmol/L, the cell viability was decreased to 82.73%. These results indicated that when the concentration of Ma-3-gal-Cl is below 10 μmol/L, it could inhibit the Aβ (1–42)/Cu^{2+}/AA system so as to induce cell apoptosis.

Scavenging effect of Ma-3-gal-Cl on OH· produced by Aβ (1–42)/Cu^{2+}/AA system

To investigate the mechanism of the protective effect of Ma-3-gal-Cl to Aβ (1–42)/Cu^{2+}/AA mixture treated cells, the scavenging effect of Ma-3-gal-Cl on OH· produced by Aβ (1–42)/Cu^{2+}/AA mixture was detected with the CCA method (61). With the increase in Ma-3-gal-Cl concentration (0, 0.5, 4, and 10 μmol/L), the amount of the OH· decreased from 100 to 20% (Figure 3). These results indicate that Ma-3-gal-Cl could inhibit the production of OH· by Aβ (1–42)/Cu^{2+}/AA mixture, and the inhibition effect is concentration-dependent.

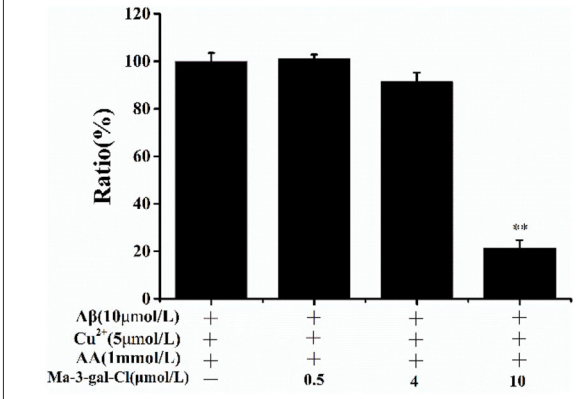

FIGURE 3
CCA fluorescence ratio of Aβ (1–42)/Cu^{2+}/AA solutions in the absence or presence of different concentrations of Ma-3-gal-Cl. $^{**}p < 0.01$ compared to values obtained in Aβ (1–42)/Cu^{2+}/AA solution.

Effects of Ma-3-gal-Cl on intracellular ROS production and mitochondrial membrane potential in Aβ (1–42)/Cu^{2+}/AA-treated SH-SY5Y cells

Intracellular ROS level is an important reflection of oxidative damage, and it can be detected with DCFH-DA (62). As shown in Figure 4A, the amount of intracellular ROS in SH-SY5Y cells incubated by Aβ (1–42)/Cu^{2+}/AA increased to 145%. With the increase in Ma-3-gal concentration (0–10 μmol/L), the amount of intracellular ROS was reduced (from 145.0 to 106.7%, compared with the control group). These results indicated that Ma-3-gal-Cl can reduce the intracellular ROS production of SH-SY5Y cells induced by Aβ (1–42)/Cu^{2+}/AA mixture.

Oxidative stress can lead to the decline of the MMP of cells and result in cell apoptosis (63, 64). To study the protective effect of Ma-3-gal-Cl on the Aβ (1–42)/Cu^{2+}/AA treated SH-SY5Y cells, the MMP was determined with JC-1 staining (42). As shown in Figure 4B, the MMP could be increased dramatically by Aβ (1–42)/Cu^{2+}/AA from 0.092 to 0.464. With the addition of Ma-3-gal-Cl, the MMP values were decreased. When the concentration of Ma-3-gal-Cl was at 4 μmol/L, the MMP value decreased to 0.356 and further increased the Ma-3-gal-Cl concentration to 10 μmol/L, and the MMP value only decreased to 0.326. These results indicated that Ma-3-gal-Cl could reduce the mitochondrial damage caused by oxidative stress from Aβ (1–42)/Cu^{2+}/AA.

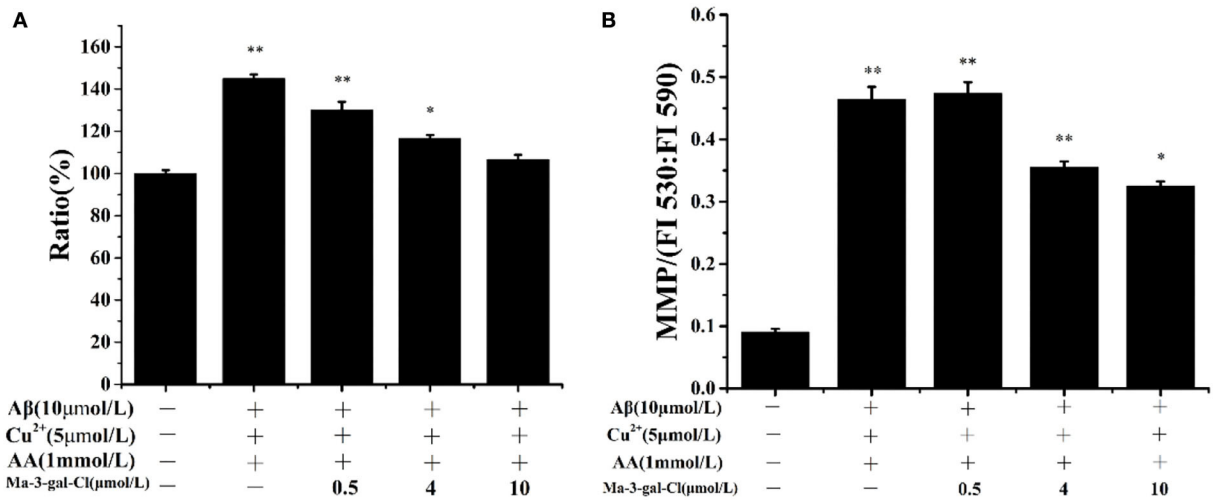

FIGURE 4
Intracellular ROS ratio **(A)** and MMP **(B)** of SH-SY5Y cells which were treated with Aβ (1–42)/Cu^{2+}/AA mixture in the absence or presence of different concentrations of Ma-3-gal-Cl. $^{*}P < 0.05$ and $^{**}p < 0.01$ compared to control values.

Effects of Ma-3-gal-Cl on expression of caspase-3 and p38 in Aβ (1–42)/Cu^{2+}/AA-treated SH-SY5Y cells

The caspase-3 and p38 are important proteins in the apoptosis pathway, and their activations can trigger a series of apoptosis reactions and lead to cell apoptosis. To investigate the molecular mechanism of the inhibition effect of Ma-3-gal-Cl to SH-SY5Y apoptosis induced by Aβ (1–42)/Cu^{2+}/AA, different concentrations (0.5, 4, and 10 μmol/L) of Ma-3-gal-Cl were selected, and the expression level of target protein was detected by Western blot (WB) assay. As shown in Figures 5A,B, the expression level of the caspase-3 (cleaved) increased in the Aβ (1–42)/Cu^{2+}/AA treated SH-SY5Y cells (from 100 to 155%), and the one for Ma-3-gal-Cl/Aβ (1–42)/Cu^{2+}/AA mixture treated cells was decreased (from 155 to 111%). As shown in Figures 5A,C, compared with the control group, the Aβ (1–42)/Cu^{2+}/AA mixture and low concentration (below 4 μmol/L) of Ma-3-gal-Cl almost have no influence on the expression of p38 in cells (Figure 5C). However, Aβ (1–42)/Cu^{2+}/AA incubation could increase the expression of P-p38 in SH-SY5Y cells. Additionally, Ma-3-gal-Cl (0–10 μmol/L) could dramatically decrease the P-p38 expression (from 300 to 108%) (Figure 5D). These results indicate that Ma-3-gal-Cl could not influence the expression of p-38 in Aβ (1–42)/Cu^{2+}/AA treated SH-SY5Y cells, but it could inhibit the expression of cleaved caspase-3 and P-p38 in Aβ (1–42)/Cu^{2+}/AA treated SH-SY5Y cells.

The inhibition effect of Ma-3-gal-Cl on Aβ (1–42) aggregation

The aggregates (oligomers, protofibrils, and fibrils) of Aβ were considered toxic species to neuron cells (65, 66). To investigate the inhibition effect of Ma-3-gal-Cl on Aβ aggregation, a ThT assay was employed. As shown in Figure 6, line A, in the first 6 h, the fluorescent intensity of the Aβ (1–42) solution increased slowly. When the incubation time is at the range of 6–48 h, the fluorescent intensity increased sharply, and the one for the longer incubation time (48–96 h) increased gradually again. These results are consistent with other reports (67–69). The lag phase (ca. 6 h) is indicative of the nucleation phase for Aβ (1–42) aggregation, whereas the fluorescent intensity plateau (48–96 h) corresponds to the formation of well-ordered, β-sheet-rich Aβ (1–42) fibrils. When the Ma-3-gal-Cl was incubated with Aβ (1–42), the fluorescent intensity of ThT increased gradually at the first 6 h and decreased at later times (Figure 6, line B). These results indicated that Ma-3-gal-Cl could inhibit the aggregation of Aβ (1–42) at the long incubation time, but could not completely inhibit Aβ (1–42) aggregation in the early hours of the incubation.

To investigate the morphology of products from the Aβ (1–42) and Ma-3-gal-Cl/Aβ (1–42) mixture, the atomic force microscope (AFM) was employed. In the Aβ (1–42) solutions, globular aggregates and short protofibrils were observed in the 3-h-incubation sample (cf. images juxtaposed in row A of Figure 7), which is consistent with the lag phase in Figure 6. After 6 h, more protofibrils were produced, and after 24 h, mature Aβ (1–42) fibrils were dominated. In the presence

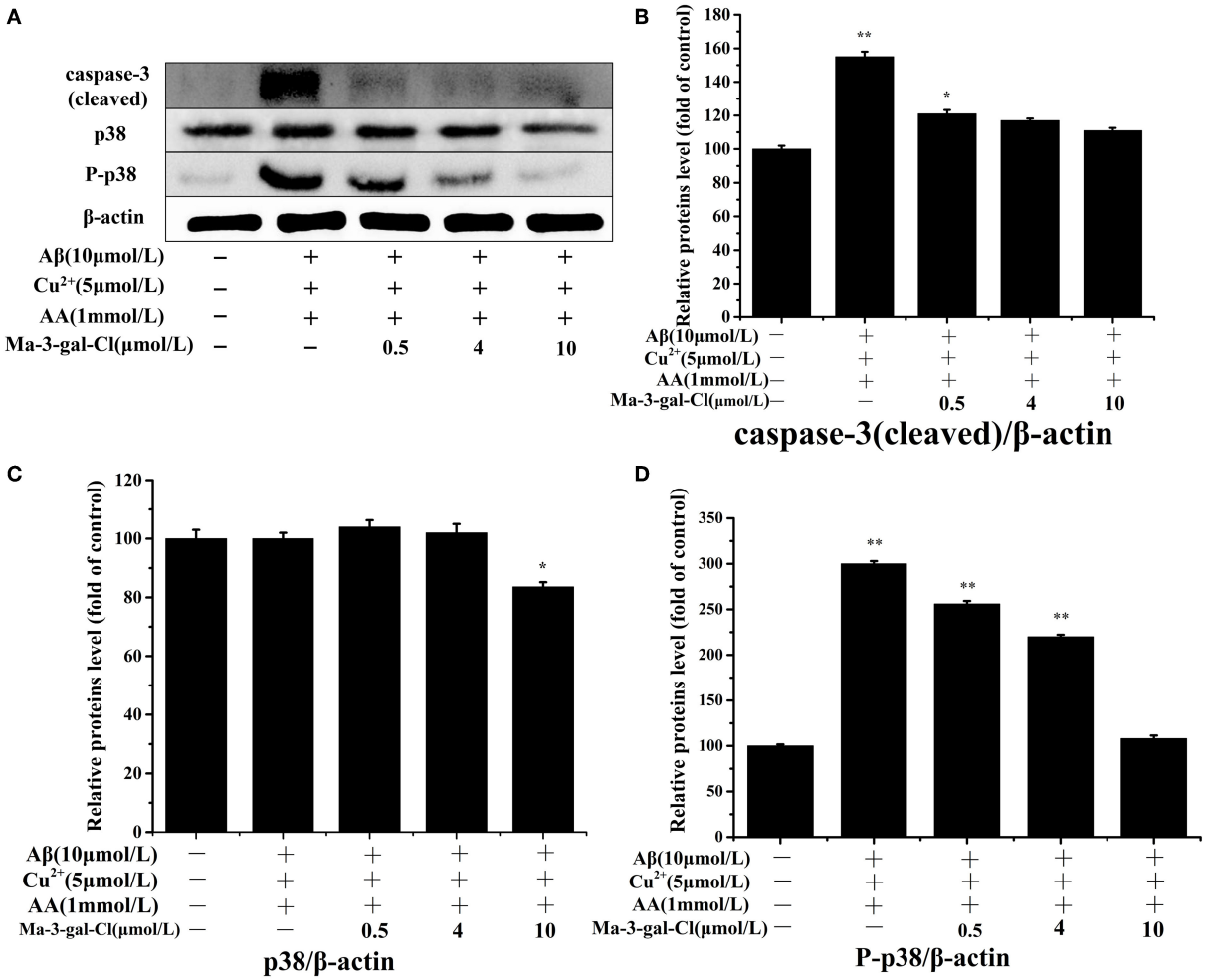

FIGURE 5
Western blot results **(A)** and effect of Ma-3-gal-Cl on the expression of caspase-3 (cleaved) **(B)**, p38 **(C)**, and P-p38 **(D)** in pretreated SH-SY5Y cells. *$P < 0.05$ and **$p < 0.01$ compared to control values.

of Ma-3-gal-Cl, at the first 6 h, the morphology of the Aβ (1–42) aggregates (Figure 7, row B) was similar to those in Aβ (1–42) alone solution (Figure 7, row A), but at 12 h, the density of Aβ (1–42) fibrils was decreased and after 24 h, the mature fibrils could not be observed, and instead with short, small aggregates. At 96 h, the amount of the small aggregates dramatically decreased. These results were consistent with ThT fluorescence results (Figure 6). This observation suggested that Ma-3-gal-Cl could bind with the Aβ (1–42) monomer and large oligomers to prevent Aβ (1–42) oligomers and protofibrils from further growing into mature fibrils.

The molecular docking results and analysis

In order to explore the specific structural basis and molecular mechanism of antioxidant and anti-aggregation effects of Ma-3-gal-Cl to Aβ (1–42), the molecular docking method was employed for further study. In the *in vitro* tests, the expressions of activated caspase-3 and P-p38 of Ma-3-gal-Cl/Aβ (1–42)/Cu^{2+}/AA mixture treated cells were decreased (Figure 5). The Aβ (1–42) aggregates were also inhibited by Ma-3-gal-Cl (Figures 6, 7). Thus, the unactivated caspase-3 (crystal structure of 2J33), mitogen-activated protein kinase kinases-6 (MKK6) (PDB ID: 3VN9) related with the active process of p-38, Aβ monomer (PDB ID: 1IYT), and fibril (PDB ID: 2BEG) were selected as receptors for the molecular docking experiments.

The structure-based docking of unactivated caspase-3, MKK6, Aβ (1–42) monomer, and fibril with Ma-3-gal-Cl gave the best score of −7.12, −7.68, −5.51, and −6.52 kCal/mol, respectively. Their interactions were visualized in 2D and 3D diagrams, and the hydrogen bond interactions between Ma-3-gal-Cl and the active site residues were observed (Figure 8). When processing the docking caspase-3 with Ma-3-gal-Cl, we first made a self-docking using the ligand in the crystal structure.

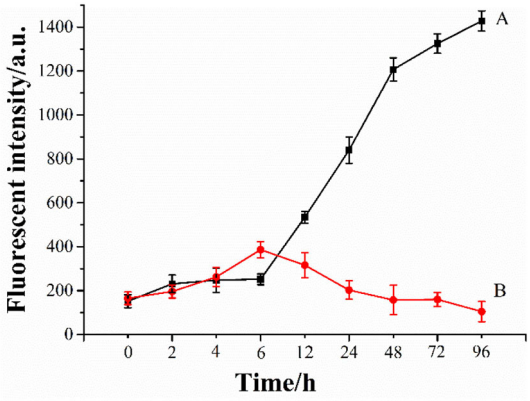

FIGURE 6
ThT fluorescence intensity of Aβ (1–42) (80 μmol/L) (A) and Aβ (1–42) (80 μmol/L)/Ma-3-gal-Cl (10 μmol/L) (B) mixture at different time.

The RMSD between the best pose and the original ligand is 1.41 Å, which indicated a set of proper docking parameters for this system. By using this set of parameters, we found that the residues, namely Cys163 (bond length: 3.60 Å), Ser120 (bond length: 2.92 Å), Arg207 (bond length: 2.77 Å), Arg64 (bond length: 2.96 Å), and Arg207 (bond length: 3.00 Å), were observed to form five hydrogen bonds with Ma-3-gal-Cl of the caspase-3 receptor (Figures 8A,E,I). For MKK6, Ma-3-gal-Cl was docked to the ATP binding site which indicated an ATP-site-directed inhibitor (70, 71). The residues, namely Ala63 (bond length: 3.20 Å), Asn184 (bond length: 2.95 Å), Asp197 (bond length: 3.03 Å), and Lys82 (bond length: 2.88 Å), were observed to form four hydrogen bonds (Figures 8B,F,J). Ma-3-gal-Cl could stay at the site with a good pose. For Aβ (1–42) monomer, there were no obvious pockets with good geometry and hydrophobicity because of no complex secondary structures. However, we found that most of the retained 10 poses tended to interact with N-terminus residues (3–17), while the importance of the N-terminal residues has been indicated in oligomerization and neurotoxicity (72, 73). In addition, these regions are the essential components of the binding site for glycosaminoglycans, which affects the change in Aβ (1–42) secondary structure from a soluble α-helix conformation to a stable β-sheet one. In the best pose, a hydrogen bond (Glu11) and a pi–H interaction (Glu3) (Figures 8C,G,K) were observed. For Aβ (1–42) fibril, the NMR structure gives important information about the identification of interaction regions, which might be targeted by inhibitor compounds. It suggested specific structural properties to interact and destabilize Aβ (1–42) self-assembly, including (a) the hydrophilic region caused by electrostatic interaction between Asp23-Lys28, (b) the Glu22 ladder formed by the Glu22 residue side chains of adjacent β-sheets, (c) the central cleft in the interior of the U-shaped turn, and (d) the hydrophobic regions caused by Leu17-Ala21 and Ala30-Val36 residues, respectively. The best pose in our study occupied the central cleft in the interior of the U-shaped turn and formed two pi–H interactions (Ala21 and Glu22), which was in line with the proposed features (Figures 8D,H,L). In addition, three poses from the 10 retained ones tended to form pi–H interactions with Glu22, Phe19, and Phe20. This can be corroborated from the side by a recent study, which indicated the π-π interactions of inhibitor agents with Phe19 and Phe20 residues can stabilize the fibrils by a reduction in the total energy of the conformation (74).

The docking results indicate that Ma-3-gal-Cl could interact with unactivated caspase-3, MKK6, Aβ (1–42) monomer, and fibril. Although there were differences in scores and interactions, there was a relatively high degree of agreement with the evidence provided by published studies. Furthermore, the calculated results accord with the experiments, which reflected our reasonable hypothesis that Ma-3-gal-Cl could reduce neuronal apoptosis by combining antioxidation and anti-aggregation of Aβ (1–42).

Discussion

A key step in exploring the active ingredients of bilberry by using cheminformatics methods is how to narrow the scope by using the basic physical and chemical properties and ADMET properties, so as to obtain the top-ranked compounds for further study. In fact, this rule should be customized according to different projects and purposes, and of no fixed pattern. In this work: (1) the molecular size was restricted because too small molecules often have no specificity; (2) the synthesizability was considered. If the synthesis is too easy, the molecule is often too simple. If the synthesis is too difficult, it is often not enough economy and feasibility. (3) Restricting indicators related to toxicity is to meet the potential of a drug. (4) Defined the commonly seen structural descriptors, including hydrogen bonds, rings and bonds, and logP, so that they will conform to the drug-likeness. (5) In general, specific and strict ADMET screening rules are usually used in drug optimization or specific aim. In the preliminary activity explore of food ingredients, it is appropriate to limit only the basic physical and chemical properties and toxicity.

According to these cheminformatics approaches, Ma-3-gal-Cl was screened from bilberry. Meanwhile, cheminformatics results also suggested Ma-3-gal-Cl could interact with Aβ. Owing to that the oxidative stress induced by the Aβ-Cu^{2+} complex and the toxic Aβ aggregates could induce neuron apoptosis and further induce AD, the effects of Ma-3-gal-Cl on these two pathways related to Aβ were investigated with *in vitro* studies.

Before the experimental investigation, we also evaluated the ability to penetrate across the blood–brain barrier (BBB) of Ma-3-gal-Cl. Ionic drugs usually need the assistance of

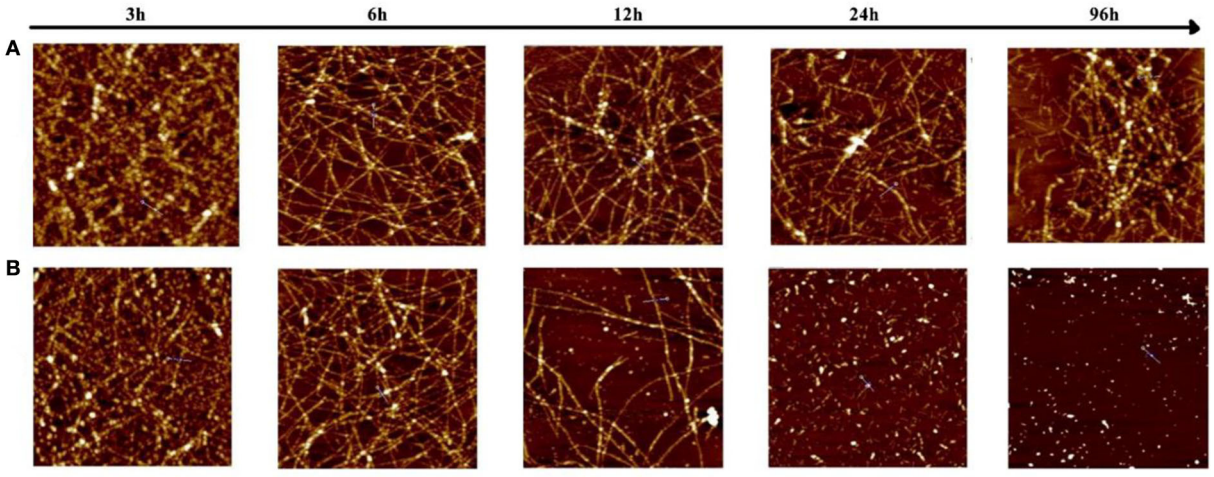

FIGURE 7
Atomic force microscopy (AFM) images of samples taken from an 80 μmol/L Aβ (1–42) solution **(A)** and Aβ (1–42) (80 μmol/L)/Ma-3-gal-Cl (10 μmol/L) mixture **(B)** at different incubation times. The scale is 2 × 2 μm.

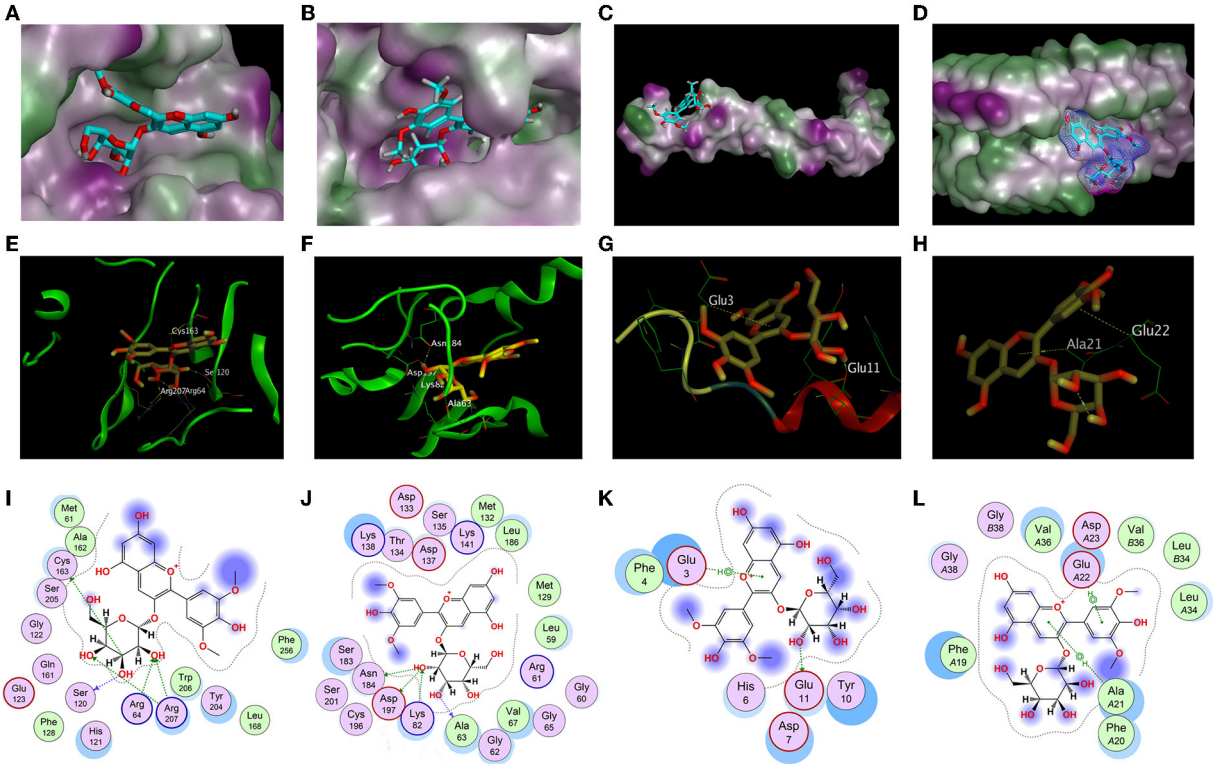

FIGURE 8
Docking results of Ma-3-gal-Cl. **(A,E,I)** The best binding pose, side view, and interaction graph of Ma-3-gal-Cl docked into the crystal structure of caspase-3 (PDB ID: 2J33). **(B,F,J)** The best binding pose, site view, and interaction graph of Ma-3-gal-Cl docked into the crystal structure of MKK6 (PDB ID: 3VN9). **(C,G,K)** The best binding pose, site view, and interaction graph of Ma-3-gal-Cl docked into the crystal structure of Aβ (1–42) monomer (PDB ID: 1IYT). **(D,H,L)** The best binding pose, side view, and interaction graph of Ma-3-gal-Cl docked into the crystal structure of Aβ (1–42) fibril (PDB ID: 2BEG).

transporters to pass through the blood–brain barrier (75–77). Referring to the method of Liu (78), we investigated the possibility of Ma-3-gal-Cl transit through the neural high-affinity chord transporter 1 (ChT1). They used the homology model based on the template of (vSGLT) because of the absence of crystal structure of ChT1 at that time. Here, based on the latest crystal structure predicted by AlphaFold, we used MOE software to evaluate the binding possibility between Ma-3-gal-Cl and BBB-ChT1 using rigid docking and semi-flexible docking (induced fit), respectively. The results showed that the binding energies of rigid and semi-flexible docking with the best scoring conformation were −7.8651 and −8.3885 kCal/mol, respectively, which indicated a potential penetrate across the BBB compared with the commonly used threshold (77, 78).

According to the *in vitro* experimental results, we believe that Ma-3-gal-Cl has the inhibition effect on Aβ/Cu^{2+}/AA induced SH-SY5Y cell apoptosis, which is mainly caused by antioxidation and anti-Aβ aggregation process. In the brain of patients with AD, aggregated Aβ and the excess amount of Cu^{2+} (∼0.4 mmol/L) were found in the senile plaque (79, 80). The toxic Aβ aggregates and oxidative stress produced by the Aβ/Cu^{2+} mixture/complex have been suggested to play an important role in AD pathogenesis (59).

As reported that the Cu^{2+} can strongly bind with Aβ peptides and the resultant complexes can facilitate the generation of H_2O_2 by reacting with cellular species such as AA and O_2 (56):

$$\begin{aligned}&\text{Ascorbic Acid} + 2\text{A}\beta - Cu^{2+} \\ &+H_2O \rightarrow \text{Dehydroascorbic acid} + 2H^+ + 2\text{A}\beta - Cu^+ \quad (3)\end{aligned}$$

$$2\text{A}\beta - Cu^+ + O_2 + 2H^+ \rightarrow 2\text{A}\beta - Cu^{2+} + H_2O_2 \quad (4)$$

In the cellular milieu, any rogue Cu^{2+} that is not readily complexed by Aβ will also react with H_2O_2 to produce hydroxyl radicals *via* Harber–Weiss reaction as (81):

$$H_2O_2 + Cu^{2+} \rightarrow Cu^+ \cdot O_2H\cdot + H^+ \quad (5)$$

$$Cu^+ \cdot O_2H\cdot + H_2O_2 \rightarrow Cu^+ + O_2 + OH^{\cdot} + H_2O \quad (6)$$

$$H^+ + Cu^+ + H_2O_2 \rightarrow Cu^{2+} + OH^{\cdot} + H_2O \quad (7)$$

As shown in our work, Aβ (1–42)/Cu^{2+}/AA system produced the hydroxyl radicals (Figure 3). The Ma-3-gal-Cl could inhibit the hydroxyl radical production and protect the SH-SY5Y cells from the oxidation damage induced by hydroxyl radicals (Figure 3). The amount of intracellular ROS and mitochondrial membrane potential in SH-SY5Y cells incubated with Aβ (1–42)/Cu^{2+}/AA system were reduced by the Ma-3-gal-Cl treatment (Figure 4). The cell apoptosis of SH-SY5Y induced by the H_2O_2 or Aβ (1–42)/Cu^{2+}/AA system was also inhibited by the Ma-3-gal-Cl treatment (Figure 2). Similar results were obtained by Kim et al. (82). In their study, three anthocyanin compounds extracted from black soybean (cyanidin-3-*O*-glucoside, delphinidin-3-*O*-glucoside, and petunidin-3-*O*-glucoside) were found could reduce the cytotoxicity of H_2O_2 to SK-N-SH cells and decrease intracellular ROS level. The antioxidant property of the anthocyanin compounds may be due to the phenolic hydroxyl groups (83).

The caspase family plays a key role in cellular apoptosis induced by oxidative damage and Aβ aggregates injury (84, 85). Caspase-3 is one of the most important downstream caspases in the apoptotic pathway, but the pro-caspase-3 has no activity in inducing cell apoptosis, while the cleaved caspase-3 has the activity. In our study, Ma-3-gal-Cl could bind with pro-caspase-3 (unactivated) (Figure 8) and inhibit the expression of cleaved caspase-3 (activated) (Figure 5).

Mitogen-activated protein kinase (MAPK) plays an important role in cell apoptosis, and the p38MAPK signaling pathway is responsible for transducing inflammatory signals and initiating apoptosis induced by oxidative damage and Aβ aggregates injury (86, 87). In the Alzheimer's disease (AD) brain, increased levels of phosphorylated (active) p38 were detected relative to age-matched normal brain (88), and the MKK6 is the main kinase for the phosphorylation process of p-38. In our study, Ma-3-gal-Cl was docked to the ATP binding site in MKK6 (Figure 8), which could inhibit the activity of MKK6 and reduced the amount of the phosphorylated (active) p38 (Figure 5).

In the senile plaque of the AD brain, aggregated Aβ is the main constituent (89). The Aβ aggregates, self-assembled from misfolded Aβ peptides, affect the structure and functions of neural cells and stimulate cell apoptosis, leading to synaptic dysfunction and neurodegeneration (89). Thus, short peptides (90), drugs (91), and natural compounds (92) were employed for inhibiting the Aβ aggregation and further inhibiting the cell toxicities. In our study, Ma-3-gal-Cl could bind with the Aβ monomer and fibrils (Figure 8), but the Ma-3-gal-Cl could bind with the N-terminal of the Aβ monomer (Figure 8), which could not inhibit Aβ aggregation at the early stage and resulted in the increase in ThT fluorescence intensity (Figure 6) and the formation of the aggregates (Figure 7) in the first 6 h. For the Aβ fibril, Ma-3-gal-Cl could bind with the U-shaped turn section of Aβ and formed pi–H interaction with Glu22, Phe19, Phe20, and Ala21 (Figure 8). These interactions of Ma-3-gal-Cl with Aβ fibril could inhibit the other Aβ aggregates (e.g., oligomers and protofibrils) and Aβ monomers to attach the formed Aβ fibrils and inhibit the further aggregation of Aβ. Thus, when the Aβ was incubated with Ma-3-gal-Cl after 6 h, the ThT fluorescence intensity was decreased (Figure 6) and the amount of Aβ aggregates was also decreased (Figure 7).

Neurodegenerative disease is a complex and multi-factorial disease, so the development of multi-target drugs for the prevention and delay of neurodegenerative disease is giving more hope (93–95). Therefore, this study attempts to explain the inhibition effect of Ma-3-gal-Cl on Aβ (1–42)/Cu^{2+}/AA system

resulting in SH-SY5Y cell apoptosis from the mechanism of antioxidation and inhibition of Aβ aggregation as follows: (1) Ma-3-gal-Cl could reduce the generation of intracellular ROS and maintain the mitochondrial membrane potential of Aβ (1–42)/Cu^{2+}/AA treated cells *via* the decreased amount of hydroxyl radicals which produced by Aβ (1–42)/Cu^{2+}/AA mixture. (2) Ma-3-gal-Cl could bind with the unactivated caspase-3 and the MKK6 to reduce the amount of activated caspase-3 and the phosphorylated p38 which induced by the Aβ (1–42)/Cu^{2+}/AA system. (3) Ma-3-gal-Cl could bind with the Aβ monomer and fibrils to inhibit the Aβ aggregation (Figure 7).

Conclusion

In this study, an effective Ma-3-gal-Cl was screened from bilberry with cheminformatics methods, and the activity and possible mechanism of the protective effect of Ma-3-gal-Cl to Aβ (1–42)/Cu^{2+}/AA treated SH-SY5Y cells were investigated with *in vitro* experiments and *in silico* calculation. The experimental results showed that Ma-3-gal-Cl had effective protection for SH-SY5Y cells treated with Aβ (1–42)/Cu^{2+}/AA by antioxidation and anti-Aβ aggregation effects. The molecular docking results provided detailed structure-based information for elucidating the multiple potential effects of Ma-3-gal-Cl against AD. Our findings suggested that Ma-3-gal-Cl could be a promising ingredient for drug development or dietary therapy for Alzheimer's disease.

Data availability statement

The original contributions presented in the study are included in the article/Supplementary material, further inquiries can be directed to the corresponding author.

Author contributions

RX: investigation, data curation, formal analysis, visualization, and writing—original draft. RL: visualization. Y-hC: validation. JD: software and writing—reviewing and editing. LZ: conceptualization, methodology, supervision, project administration, and funding acquisition. All authors contributed to the article and approved the submitted version.

Funding

This study was supported by the Science and Technology Innovation Program of Hunan Province (2022RC1148), the Natural Science Foundation of Hunan Province of China (2022JJ31009 and 2022JJ50260), the Natural Science Foundation of Changsha (kq2202282), and a Program for Science and Technology of Education Department of Hunan Province (20B620).

Conflict of interest

Author RX was employed by Sinocare Inc.

The remaining authors declare that the research was conducted in the absence of any commercial or financial relationships that could be construed as a potential conflict of interest.

Publisher's note

All claims expressed in this article are solely those of the authors and do not necessarily represent those of their affiliated organizations, or those of the publisher, the editors and the reviewers. Any product that may be evaluated in this article, or claim that may be made by its manufacturer, is not guaranteed or endorsed by the publisher.

Supplementary material

The Supplementary Material for this article can be found online at: https://www.frontiersin.org/articles/10.3389/fnut.2022.1061552/full#supplementary-material

References

1. Qian X, Hamad B, Dias-Lalcaca G. The Alzheimer disease market. *Nat Rev Drug Discov.* (2015) 14:675–6. doi: 10.1038/nrd4749

2. Forstl H, Kurz A. Clinical features of Alzheimer's disease. *Eur Arch Psychiatry Clin Neurosci.* (1999) 249:288–90. doi: 10.1007/s004060050101

3. Hardy JA, Higgins GA. Alzheimer's disease: the amyloid cascade hypothesis. *Science.* (1992) 256:184–5. doi: 10.1126/science.1566067

4. Korsak M, Kozyreva T. Beta amyloid hallmarks: from intrinsically disordered proteins to Alzheimer's disease. *Adv Exp Med Biol.* (2015) 870:401–21. doi: 10.1007/978-3-319-20164-1_14

5. Garai K, Sengupta P, Sahoo B, Maiti S. Selective destabilization of soluble amyloid beta oligomers by divalent metal ions. *Biochem Biophys Res Commun.* (2006) 345:210–5. doi: 10.1016/j.bbrc.2006.04.056

6. Akanji MA, Rotimi DE, Elebiyo TC, Awakan OJ, Adeyemi OS. Redox homeostasis and prospects for therapeutic targeting in neurodegenerative disorders. *Oxid Med Cell Longev.* (2021) 2021:9971885. doi: 10.1155/2021/9971885

7. Su XY, Wu WH, Huang ZP, Hu J, Lei P, Yu CH, et al. Hydrogen peroxide can be generated by tau in the presence of Cu(II). *Biochem Biophys Res Commun.* (2007) 358:661–5. doi: 10.1016/j.bbrc.2007.04.191

8. Lovell MA, Robertson JD, Teesdale WJ, Campbell JL, Markesbery WR. Copper, iron and zinc in Alzheimer's disease senile plaques. *J Neurol Sci.* (1998) 158:47–52. doi: 10.1016/s0022-510x(98)00092-6

9. Schneider LS. Introducing Alzheimer's & Dementia: Translational Research & Clinical Interventions, an open access journal of the Alzheimer's Association. *Alzh Dement-Trci.* (2015) 1:91–3. doi: 10.1016/j.trci.2015.06.002

10. Dey A, Bhattacharya R, Mukherjee A, Pandey DK. Natural products against Alzheimer's disease: pharmaco-therapeutics and biotechnological interventions. *Biotechnol Adv.* (2017) 35:178–216. doi: 10.1016/j.biotechadv.2016.12.005

11. Noori T, Dehpour AR, Sureda A, Sobarzo-Sanchez E, Shirooie S. Role of natural products for the treatment of Alzheimer's disease. *Eur J Pharmacol.* (2021) 898:173974. doi: 10.1016/j.ejphar.2021.173974

12. Espin JC, Soler-Rivas C, Wichers HJ, Garcia-Viguera C. Anthocyanin-based natural colorants: a new source of antiradical activity for foodstuff. *J Agric Food Chem.* (2000) 48:1588–92. doi: 10.1021/jf9911390

13. Sun LL, Gao W, Zhang MM Li C, Wang AG, Su YL, et al. Composition and antioxidant activity of the anthocyanins of the fruit of Berberis heteropoda Schrenk. *Molecules.* (2014) 19:19078–96. doi: 10.3390/molecules191119078

14. Li D, Wang P, Luo Y, Zhao M, Chen F. Health benefits of anthocyanins and molecular mechanisms: update from recent decade. *Crit Rev Food Sci Nutr.* (2017) 57:1729–41. doi: 10.1080/10408398.2015.1030064

15. Miguel MG. Antioxidant and anti-inflammatory activities of essential oils: a short review. *Molecules.* (2010) 15:9252–87. doi: 10.3390/molecules15129252

16. Phan MA, Bucknall MP, Arcot J. Interferences of anthocyanins with the uptake of lycopene in Caco-2 cells, and their interactive effects on anti-oxidation and anti-inflammation in vitro and ex vivo. *Food Chem.* (2019) 276:402–9. doi: 10.1016/j.foodchem.2018.10.012

17. Afzal M, Redha A, AlHasan R. Anthocyanins potentially contribute to defense against Alzheimer's disease. *Molecules.* (2019) 24:4255. doi: 10.3390/molecules24234255

18. Shukitt-Hale B, Bielinski DF, Lau FC, Willis LM, Carey AN, Joseph JA. The beneficial effects of berries on cognition, motor behavior and neuronal function in ageing. *Br J Nutr.* (2015) 114:1542–9. doi: 10.1017/S0007114515003451

19. Chen Y, Kirchmair J. Cheminformatics in natural product-based drug discovery. *Mol Inform.* (2020) 39:e2000171. doi: 10.1002/minf.202000171

20. Dong J, Wang NN, Yao ZJ, Zhang L, Cheng Y, Ouyang D, et al. ADMETlab: a platform for systematic ADMET evaluation based on a comprehensively collected ADMET database. *J Cheminform.* (2018) 10:29. doi: 10.1186/s13321-018-0283-x

21. Yao Z-J, Dong J, Che Y-J, Zhu M-F, Wen M, Wang N-N, et al. TargetNet: a web service for predicting potential drug-target interaction profiling via multi-target SAR models. *J Comput Aided Mol Des.* (2016) 30:413–24. doi: 10.1007/s10822-016-9915-2

22. Yang Z-F, Xiao R, Xiong G-L, Lin Q-L, Liang Y, Zeng W-B, et al. A novel multi-layer prediction approach for sweetness evaluation based on systematic machine learning modeling. *Food Chem.* (2022) 372:131249. doi: 10.1016/j.foodchem.2021.131249

23. Yu H-D, Qing L-W, Yan D-T, Xia G, Zhang C, Yun Y-H, et al. Hyperspectral imaging in combination with data fusion for rapid evaluation of tilapia fillet freshness. *Food Chem.* (2021) 348:129129. doi: 10.1016/j.foodchem.2021.129129

24. Ma P, Zhang Z, Li Y, Yu N, Sheng J, Küçük McGinty H, et al. Deep learning accurately predicts food categories and nutrients based on ingredient statements. *Food Chem.* (2022) 391:133243. doi: 10.1016/j.foodchem.2022.133243

25. Chen Y, Qian J, Liang R, Zeng W-B, Dong J, Lin Q-L. Precise Hapten design of sulfonamides by combining machine learning and 3D-QSAR approaches. *Food Anal Methods.* (2022) 15:1085–97. doi: 10.1007/s12161-021-02179-x

26. Goel A, Gajula K, Gupta R, Rai B. In-silico screening of database for finding potential sweet molecules: a combined data and structure based modeling approach. *Food Chem.* (2021) 343:128538. doi: 10.1016/j.foodchem.2020.128538

27. Yu Z, Fan Y, Zhao W, Ding L, Li J, Liu J. Novel angiotensin-converting enzyme inhibitory peptides derived from Oncorhynchus mykiss Nebulin: virtual screening and in silico molecular docking study. *J Food Sci.* (2018) 83:2375–83. doi: 10.1111/1750-3841.14299

28. Dong J, Cao D-S, Miao H-Y, Liu S, Deng B-C, Yun Y-H, et al. ChemDes: an integrated web-based platform for molecular descriptor and fingerprint computation. *J Cheminform.* (2015) 7:60. doi: 10.1186/s13321-015-0109-z

29. Dong J, Yao Z-J, Zhang L, Luo F, Lin Q, Lu A-P, et al. PyBioMed: a python library for various molecular representations of chemicals, proteins and DNAs and their interactions. *J Cheminform.* (2018) 10:16. doi: 10.1186/s13321-018-0270-2

30. Xiong G, Wu Z, Yi J, Fu L, Yang Z, Hsieh C, et al. ADMETlab 20: an integrated online platform for accurate and comprehensive predictions of ADMET properties. *Nuc Acids Res.* (2021) 49:W5–W14. doi: 10.1093/nar/gkab255

31. Forouzesh A, Samadi Foroushani S, Forouzesh F, Zand E. reliable target prediction of bioactive molecules based on chemical similarity without employing statistical methods. *Front Pharmacol.* (2019) 10:835. doi: 10.3389/fphar.2019.00835

32. Daina A, Michielin O, Zoete V. Swiss target prediction: updated data and new features for efficient prediction of protein targets of small molecules. *Nucleic Acids Res.* (2019) 47:W357–64. doi: 10.1093/nar/gkz382

33. Awale M, Reymond JL. Polypharmacology Browser PPB2: target prediction combining nearest neighbors with machine learning. *J Chem Inf Model.* (2019) 59:10–7. doi: 10.1021/acs.jcim.8b00524

34. Liu X, Ouyang S, Yu B, Liu Y, Huang K, Gong J, et al. PharmMapper server: a web server for potential drug target identification using pharmacophore mapping approach. *Nucleic Acids Res.* (2010) 38:W609–14. doi: 10.1093/nar/gkq300

35. Wang X, Shen Y, Wang S, Li S, Zhang W, Liu X, et al. PharmMapper 2017 update: a web server for potential drug target identification with a comprehensive target pharmacophore database. *Nucleic Acids Res.* (2017) 45:W356–60. doi: 10.1093/nar/gkx374

36. Dunkel M, Günther S, Ahmed J, Wittig B, Preissner R. SuperPred: drug classification and target prediction. *Nucleic Acids Res.* (2008) 36:W55–9. doi: 10.1093/nar/gkn307

37. Nickel J, Gohlke BO, Erehman J, Banerjee P, Rong WW, Goede A, et al. SuperPred: update on drug classification and target prediction. *Nucleic Acids Res.* (2014) 42:W26–31. doi: 10.1093/nar/gku477

38. Kim MJ, Kim JH, Kim JH, Lee S, Cho EJ. Amelioration effects of Cirsium japonicum var. maackii extract/fractions on amyloid beta25-35-induced neurotoxicity in SH-SY5Y cells and identification of the main bioactive compound. *Food Funct.* (2020) 11:9651–61. doi: 10.1039/d0fo01041c

39. Fu QQ, Wei L, Sierra J, Cheng JZ, Moreno-Flores MT, You H, et al. Olfactory Ensheathing cell-conditioned medium reverts Aβ25-35-induced oxidative damage in SH-SY5Y cells by modulating the mitochondria-mediated apoptotic pathway. *Cell Mol Neurobiol.* (2017) 37:1043–54. doi: 10.1007/s10571-016-0437-1

40. Wang K, Zhu L, Zhu X, Zhang K, Huang B, Zhang J, et al. Protective effect of paeoniflorin on Aβ25-35-induced SH-SY5Y cell injury by preventing mitochondrial dysfunction. *Cell Mol Neurobiol.* (2014) 34:227–34. doi: 10.1007/s10571-013-0006-9

41. Cheignon C, Jones M, Atrián-Blasco E, Kieffer I, Faller P, Collin F, et al. Identification of key structural features of the elusive Cu-Aβ complex that generates ROS in Alzheimer's disease. *Chem Sci.* (2017) 8:5107–18. doi: 10.1039/c7sc00809k

42. Cheng W, Chen W, Wang P, Chu J. Asiatic acid protects differentiated PC12 cells from Aβ25-35-induced apoptosis and tau hyperphosphorylation via regulating PI3K/Akt/GSK-3β signaling. *Life Sci.* (2018) 208:96–101. doi: 10.1016/j.lfs.2018.07.016

43. Lovas S, Zhang Y, Yu J, Lyubchenko YL. Molecular mechanism of misfolding and aggregation of Aβ (13-23). *J Phys Chem B.* (2013) 117:6175–86. doi: 10.1021/jp402938p

44. Legleiter J, Czilli DL, Gitter B, DeMattos RB, Holtzman DM, Kowalewski T. Effect of different anti-Abeta antibodies on Abeta fibrillogenesis as assessed by atomic force microscopy. *J Mol Biol.* (2004) 335:997–1006. doi: 10.1016/j.jmb.2003.11.019

45. Feeney B, Pop C, Swartz P, Mattos C, Clark AC. Role of loop bundle hydrogen bonds in the maturation and activity of (Pro)caspase-3. *Biochemistry.* (2006) 45:13249–63. doi: 10.1021/bi0611964

46. Matsumoto T, Kinoshita T, Matsuzaka H, Nakai R, Kirii Y, Yokota K, et al. Crystal structure of non-phosphorylated MAP2K6 in a putative auto-inhibition state. *J Biochem.* (2012) 151:541–9. doi: 10.1093/jb/mvs023

47. Crescenzi O, Tomaselli S, Guerrini R, Salvadori S, D'Ursi AM, Temussi PA, et al. Solution structure of the Alzheimer amyloid beta-peptide (1-42) in an apolar microenvironment. Similarity with a virus fusion domain. *Eur J Biochem.* (2002) 269:5642–8. doi: 10.1046/j.1432-1033.2002.03271.x

48. Luhrs T, Ritter C, Adrian M, Riek-Loher D, Bohrmann B, Dobeli H, et al. 3D structure of Alzheimer's amyloid-beta(1-42) fibrils. *Proc Natl Acad Sci U S A.* (2005) 102:17342–7. doi: 10.1073/pnas.0506723102

49. Heysieattalab S, Sadeghi L. Effects of delphinidin on pathophysiological signs of nucleus basalis of meynert lesioned rats as animal model of Alzheimer disease. *Neurochem Res.* (2020) 45:1636–46. doi: 10.1007/s11064-020-03027-w

50. Thummayot S, Tocharus C, Suksamrarn A, Tocharus J. Neuroprotective effects of cyanidin against Aβ-induced oxidative and ER stress in SK-N-SH cells. *Neurochem Int.* (2016) 101:15–21. doi: 10.1016/j.neuint.2016.09.016

51. Chen S, Zhou H, Zhang G, Meng J, Deng K, Zhou W, et al. Anthocyanins from Lycium ruthenicum Murr. Ameliorated d-Galactose-Induced Memory Impairment, Oxidative Stress, and Neuroinflammation in adult rats. *J Agric Food Chem.* (2019) 67:3140–9. doi: 10.1021/acs.jafc.8b06402

52. Sabogal-Guáqueta AM, Muñoz-Manco JI, Ramírez-Pineda JR, Lamprea-Rodriguez M, Osorio E, Cardona-Gómez GP. The flavonoid quercetin ameliorates Alzheimer's disease pathology and protects cognitive and emotional function in aged triple transgenic Alzheimer's disease model mice. *Neuropharmacology.* (2015) 93:134–45. doi: 10.1016/j.neuropharm.2015.01.027

53. Jabir NR, Khan FR, Tabrez S. Cholinesterase targeting by polyphenols: A therapeutic approach for the treatment of Alzheimer's disease. *CNS Neurosci Ther.* (2018) 24:753–62. doi: 10.1111/cns.12971

54. Xicota L, Rodriguez-Morato J, Dierssen M, La Torre R de. Potential Role of (-)-Epigallocatechin-3-Gallate (EGCG) in the secondary prevention of Alzheimer disease. *Curr Drug Targets.* (2017) 18:174–95. doi: 10.2174/1389450116666150825113655

55. Wang B, Zhong Y, Gao C, Li J. Myricetin ameliorates scopolamine-induced memory impairment in mice via inhibiting acetylcholinesterase and down-regulating brain iron. *Biochem Biophys Res Commun.* (2017) 490:336–42. doi: 10.1016/j.bbrc.2017.06.045

56. Huang X, Atwood CS, Hartshorn MA, Multhaup G, Goldstein LE, Scarpa RC, et al. The A beta peptide of Alzheimer's disease directly produces hydrogen peroxide through metal ion reduction. *Biochemistry.* (1999) 38:7609–16. doi: 10.1021/bi990438f

57. Yang CA, Chen YH, Ke SC, Chen YR, Huang HB, Lin TH, et al. Correlation of copper interaction, copper-driven aggregation, and copper-driven h(2)o(2) formation with aβ40 conformation. *Int J Alzheimers Dis.* (2010) 2011:607861. doi: 10.4061/2011/607861

58. Everett J, Lermyte F, Brooks J, Tjendana-Tjhin V, Plascencia-Villa G, Hands-Portman I, et al. Biogenic metallic elements in the human brain? *Sci Adv.* (2021) 7:6707. doi: 10.1126/sciadv.abf6707

59. Jiang D, Li X, Liu L, Yagnik GB, Zhou F. Reaction rates and mechanism of the ascorbic acid oxidation by molecular oxygen facilitated by Cu(II)-containing amyloid-beta complexes and aggregates. *J Phys Chem B.* (2010) 114:4896–903. doi: 10.1021/jp9095375

60. Kanti Das T, Wati MR, Fatima-Shad K. Oxidative stress gated by fenton and haber weiss reactions and its association with Alzheimer's disease. *Arch Neurosci.* (2014) 2:78. doi: 10.5812/archneurosci.20078

61. Cheignon C, Collin F, Faller P, Hureau C. Is ascorbate Dr Jekyll or Mr Hyde in the Cu(Aβ) mediated oxidative stress linked to Alzheimer's disease? *Dalton Trans.* (2016) 45:12627–31. doi: 10.1039/c6dt01979j

62. Yang L, Wang N, Zheng G. Enhanced effect of combining chlorogenic acid on selenium nanoparticles in inhibiting amyloid β aggregation and reactive oxygen species formation *in vitro*. *Nanoscale Res Lett.* (2018) 13:303. doi: 10.1186/s11671-018-2720-1

63. Zhao C, Su P, Lv C, Guo L, Cao G, Qin C, et al. Berberine alleviates amyloid β-induced mitochondrial dysfunction and synaptic loss. *Oxid Med Cell Longev.* (2019) 2019:7593608. doi: 10.1155/2019/7593608

64. Li Y, Lu J, Cao X, Zhao H, Gao L, Xia P, et al. A newly synthesized rhamnoside derivative alleviates Alzheimer's amyloid-β-induced oxidative stress, mitochondrial dysfunction, and cell senescence through upregulating SIRT3. *Oxid Med Cell Longev.* (2020) 2020:7698560. doi: 10.1155/2020/7698560

65. Walsh DM, Selkoe DJ. A beta oligomers - a decade of discovery. *J Neurochem.* (2007) 101:1172–84. doi: 10.1111/j.1471-4159.2006.04426.x

66. Wang K, Na L, Duan M. The pathogenesis mechanism, structure properties, potential drugs and therapeutic nanoparticles against the small oligomers of amyloid-β. *Curr Top Med Chem.* (2021) 21:151–67. doi: 10.2174/1568026620666200916123000

67. Fan Q, Liu Y, Wang X, Zhang Z, Fu Y, Liu L, et al. Ginnalin A Inhibits aggregation, reverses fibrillogenesis, and alleviates cytotoxicity of amyloid β (1-42). *ACS Chem Neurosci.* (2020) 11:638–47. doi: 10.1021/acschemneuro.9b00673

68. Stefanescu R, Stanciu GD, Luca A, Paduraru L, Tamba B-I. Secondary metabolites from plants possessing inhibitory properties against beta-amyloid aggregation as revealed by Thioflavin-T assay and correlations with investigations on transgenic mouse models of Alzheimer's disease. *Biomolecules.* (2020) 10:870. doi: 10.3390/biom10060870

69. Ramesh BN, Indi SS, Rao KS. Anti-amyloidogenic property of leaf aqueous extract of Caesalpinia crista. *Neurosci Lett.* (2010) 475:110–4. doi: 10.1016/j.neulet.2010.03.062

70. Kwong AJ, Scheidt KA. Non-'classical' MEKs: A review of MEK3-7 inhibitors. *Bioorg Med Chem Lett.* (2020) 30:127203. doi: 10.1016/j.bmcl.2020.127203

71. Adams M, Kobayashi T, Lawson JD, Saitoh M, Shimokawa K, Bigi SV, et al. Fragment-based drug discovery of potent and selective MKK3/6 inhibitors. *Bioorg Med Chem Lett.* (2016) 26:1086–9. doi: 10.1016/j.bmcl.2015.11.054

72. Bartolini M, Bertucci C, Bolognesi ML, Cavalli A, Melchiorre C, Andrisano V. Insight into the kinetic of amyloid beta (1-42) peptide self-aggregation: elucidation of inhibitors' mechanism of action. *Chembiochem.* (2007) 8:2152–61. doi: 10.1002/cbic.200700427

73. Williamson MP, Suzuki Y, Bourne NT, Asakura T. Binding of amyloid beta-peptide to ganglioside micelles is dependent on histidine-13. *Biochem J.* (2006) 397:483–90. doi: 10.1042/BJ20060293

74. Kumar J, Namsechi R, Sim VL. Structure-based peptide design to modulate amyloid beta aggregation and reduce cytotoxicity. *PLoS ONE.* (2015) 10:e0129087. doi: 10.1371/journal.pone.0129087

75. Banks WA. From blood-brain barrier to blood-brain interface: new opportunities for CNS drug delivery. *Nat Rev Drug Discov.* (2016) 15:275–92. doi: 10.1038/nrd.2015.21

76. Pardridge WM. Drug transport across the blood-brain barrier. *J Cereb Blood Flow Metab.* (2012) 32:1959–72. doi: 10.1038/jcbfm.2012.126

77. Shityakov S, Förster C. In silico predictive model to determine vector-mediated transport properties for the blood-brain barrier choline transporter. *Adv Appl Bioinform Chem.* (2014) 7:23–36. doi: 10.2147/AABC.S63749

78. Liu S, Cao X-L, Liu G-Q, Zhou T, Yang X-L, Ma B-X. The in silico and in vivo evaluation of puerarin against Alzheimer's disease. *Food Funct.* (2019) 10:799–813. doi: 10.1039/c8fo01696h

79. Matheou CJ, Younan ND, Viles JH. Cu^{2+} accentuates distinct misfolding of Aβ1–40 and Aβ1–4_2 peptides, and potentiates membrane disruption. *Biochem J.* (2015) 466:233–42. doi: 10.1042/BJ20141168

80. Fica-Contreras SM, Shuster SO, Durfee ND, Bowe GJ, Henning NJ, Hill SA, et al. Glycation of Lys-16 and Arg-5 in amyloid-β and the presence of Cu^{2+} play a major role in the oxidative stress mechanism of Alzheimer's disease. *J Biol Inorg Chem.* (2017) 22:1211–22. doi: 10.1007/s00775-017-1497-5

81. Barb WG Baxendale JH, George P, Hargrave KR. Reactions of Ferrous and Ferric Ions with Hydrogen Peroxide. *Nature.* (1949) 163:692–4. doi: 10.1038/163692a0

82. Kim SM, Chung MJ, Ha TJ, Choi HN, Jang SJ, Kim SO, et al. Neuroprotective effects of black soybean anthocyanins via inactivation of ASK1-JNK/p38 pathways and mobilization of cellular sialic acids. *Life Sci.* (2012) 90:874–82. doi: 10.1016/j.lfs.2012.04.025

83. Fukumoto LR, Mazza G. Assessing antioxidant and pro-oxidant activities of phenolic compounds. *J Agric Food Chem.* (2000) 48:3597–604. doi: 10.1021/jf000220w

84. Velez-Pardo C, Garcia Ospina G, Del Jimenez Rio M. Aβ[25–35] peptide and iron promote apoptosis in lymphocytes by an oxidative stress mechanism: involvement of H2O2, Caspase-3, NF-κB, p53 and c-Jun. *Neurotoxicology.* (2002) 23:351–65. doi: 10.1016/S0161-813X(02)00081-5

85. Jazvinšćak Jembrek M, Hof PR, Šimić G. Ceramides in Alzheimer's disease: key mediators of neuronal apoptosis induced by oxidative stress and Aβ accumulation. *Oxid Med Cell Longev.* (2015) 2015:346783. doi: 10.1155/2015/346783

86. Chauhan V, Chauhan A. Oxidative stress in Alzheimer's disease. *Pathophysiology.* (2006) 13:195–208. doi: 10.1016/j.pathophys.2006.05.004

87. Zhang G, Pare RB, Chin KL, Qian Y. Tβ4 ameliorates oxidative damage and apoptosis through ERK/MAPK and 5-HT1A signaling pathway in Aβ insulted SH-SY5Y cells. *Life Sci.* (2021 3):120178. doi: 10.1016/j.lfs.2021.120178

88. Hensley K, Floyd RA, Zheng NY, Nael R, Robinson KA, Nguyen X, et al. p38 kinase is activated in the Alzheimer's disease brain. *J Neurochem.* (1999) 72:2053–8. doi: 10.1046/j.1471-4159.1999.0722053.x

89. Gouras GK, Tsai J, Naslund J, Vincent B, Edgar M, Checler F, et al. Intraneuronal Aβ42 Accumulation in human brain. *Am J Pathol.* (2000) 156:15–20. doi: 10.1016/S0002-9440(10)64700-1

90. Moore BD, Martin J, Mena L de, Sanchez J, Cruz PE, Ceballos-Diaz C, et al. Short Aβ peptides attenuate Aβ42 toxicity *in vivo*. *J Exp Med.* (2018) 215:283–301. doi: 10.1084/jem.20170600

91. Yahata N, Asai M, Kitaoka S, Takahashi K, Asaka I, Hioki H, et al. Anti-Aβ drug screening platform using human iPS cell-derived neurons for the treatment of Alzheimer's disease. *PLoS One.* (2011) 6:e25788. doi: 10.1371/journal.pone.0025788

92. Bu X-L, Rao PP, Wang Y-J. Anti-amyloid aggregation activity of natural compounds: implications for Alzheimer's drug discovery. *Mol Neurobiol.* (2016) 53:3565–75. doi: 10.1007/s12035-015-9301-4

93. Nepovimova E, Korabecny J, Dolezal R, Babkova K, Ondrejicek A, Jun D, et al. Tacrine-Trolox hybrids: a novel class of centrally active, non-hepatotoxic multi-target-directed ligands exerting anticholinesterase and antioxidant activities with low *in vivo* toxicity. *J Med Chem.* (2015) 58:8985–9003. doi: 10.1021/acs.jmedchem.5b01325

94. Zha X, Lamba D, Zhang L, Lou Y, Xu C, Kang D, et al. Novel Tacrine-Benzofuran hybrids as potent multitarget-directedligands for the treatment of Alzheimer's disease: design, synthesis, biological evaluation, and X-ray crystallography. *J Med Chem.* (2016) 59:114–31. doi: 10.1021/acs.jmedchem.5b01119

95. Garcia-Font N, Hayour H, Belfaitah A, Pedraz J, Moraleda I, Iriepa I, et al. Potent anticholinesterasic and neuroprotective pyranotacrines as inhibitors of beta-amyloid aggregation, oxidative stress and tau-phosphorylation for Alzheimer's disease. *Eur J Med Chem.* (2016) 118:178–92. doi: 10.1016/j.ejmech.2016.04.023